Atmospheric
Chemistry
and Physics

Atmospheric lifetime of sulphur hexafluoride (SF$_6$) and five other trace gases in the BASCOE model driven by three reanalyses

Sarah Vervalcke[1], **Quentin Errera**[1], **Roland Eichinger**[2], **Thomas Reddmann**[3], **Simon Chabrillat**[1], **Marc Op de beeck**[1], **Gabriele Stiller**[3], and **Emmanuel Mahieu**[4]

[1]Royal Belgian Institute for Space Aeronomy (BIRA-IASB), Brussels, Belgium
[2]Institut für Physik der Atmosphäre, Deutsches Zentrum für Luft- und Raumfahrt (DLR), Oberpfaffenhofen, Germany
[3]Institute for Meteorology and Climate Research, Karlsruhe Institute of Technology (KIT), Karlsruhe, Germany
[4]Institute of Astrophysics and Geophysics, Université de Liège (ULg), Liège, Belgium

Correspondence: Sarah Vervalcke (sarah.vervalcke@aeronomie.be) and Quentin Errera
(quentin.errera@aeronomie.be)

Abstract. In this work, sulphur hexafluoride (SF$_6$), which is often used as a tracer for stratospheric transport due to its inertness in the stratosphere and nearly linear growth rate in the troposphere, is included in the chemistry transport model (CTM) of the Belgian Assimilation System for Chemical ObsErvations (BASCOE). Sink and recovery reactions for this species are implemented in the model, which has a top in the mesosphere at 0.01 hPa. The simulated SF$_6$ distributions are compared with MIPAS and ACE-FTS observations and the global atmospheric lifetime is computed from CTM runs driven by three recent meteorological reanalyses: ERA5, MERRA2 and JRA-3Q. The results show that BASCOE SF$_6$ profiles are generally within 10 % of the satellite observations below 10 hPa, although discrepancies increase at higher altitudes. The global atmospheric lifetime is used as an additional diagnostic for the implementation of the chemistry in the mesosphere, where satellite measurements are unavailable. The derived SF$_6$ lifetimes are 2646 years with ERA5, 1909 years with MERRA2 and 2147 years with JRA-3Q, in accordance with recent literature. Due to the large spread of published lifetimes for SF$_6$, the study is extended to N$_2$O, CH$_4$, CFC-11, CFC-12 and HCFC-22, to validate the SF$_6$ results. The lifetimes for these species are in agreement with previously reported values, and their spread between simulations is smaller compared to SF$_6$. This analysis highlights the sensitivity of SF$_6$ to the input reanalysis data sets and thus to differences in dynamics.

1 Introduction

Studies of middle atmospheric transport have been important for a long time and are motivated in part by the existence of the stratospheric ozone layer that protects the Earth from solar UV radiation. Transport of trace gases in the stratosphere is dominated by a large scale circulation pattern that is part of the Brewer–Dobson circulation (BDC), discovered by Alan Brewer and Gordon Dobson (Brewer, 1949; Dobson, 1956; Dobson et al., 1930). The BDC is the result of an uplift of air

from the tropical tropopause into the stratosphere and a consequent poleward transport driven by planetary wave breaking in the atmosphere. At mid- and high latitudes the air returns to the troposphere upon which it can be recirculated. The BDC is important for the transport of trace gases such as ozone, influencing both the chemistry and climate of the atmosphere. A comprehensive review of the Brewer–Dobson circulation can be found in Butchart (2014).

Climate models predict an increase in the strength of the BDC (Butchart et al., 2006; Hardiman et al., 2013; Abalos

et al., 2021), typically quantified by the tropical mass up-welling. While strength and speed describe different aspects of the circulation, they tend to vary together, as shown in Austin and Li (2006). A common way to diagnose the speed of the BDC is through age of air (AoA) studies. These studies look at the (average) time an air parcel takes to move from a reference surface in the troposphere to the strato-sphere. Changes in AoA at a given location in the strato-sphere thus reflect changes in circulation speed: the trans-portation time increases when the circulation slows down and decreases when the circulation speeds up. Additionally, two-way mixing between the tropics and the extra-tropics can in-crease stratospheric AoA by making air parcels recirculate, while in the extra-tropical lower stratosphere, mixing reju-venates the air. Mixing within the extra-tropical stratosphere also has local effects and flattens the latitudinal age gradi-ent (Garny et al., 2014; Dietmüller et al., 2018; Eichinger et al., 2019). The concept of AoA is described in Hall and Plumb (1994) and Garny et al. (2024b). The AoA can be computed from a synthetic, idealized model tracer or from real long-lived trace gases with a nearly linear increase in the troposphere, such as carbon dioxide (CO$_2$) and sulphur hexafluoride (SF$_6$). SF$_6$ in particular is often used because of its inertness in the stratosphere and the absence of strong seasonal variations. The emissions of SF$_6$ at the surface are almost completely anthropogenic due to its use in high volt-age insulation for the transmission and distribution of elec-tricity. Additionally, SF$_6$ is a potent greenhouse gas with a global warming potential that is estimated to be 22 500 times larger than that of CO$_2$ (Wang et al., 2019) and is therefore important for climate studies. However, SF$_6$ suffers from a sink reaction in the mesosphere which makes the age of air older than what is expected from an inert tracer. Moreover, SF$_6$ is a noisy data product because its spectral signatures are close to those of CO$_2$ and H$_2$O, and due to its low abundance in the atmosphere, on the order of parts per trillion, the sig-nal is weak. While this provides challenges when using SF$_6$ as a tracer of the residual circulation, Garny et al. (2024a) propose a correction for the ageing due to the mesospheric loss and Voet et al. (2025) combines several long-lived trace gases to compute the AoA, which reduces the uncertainty compared to a method based on SF$_6$ alone.

While AoA trends are a useful diagnostic, discrepan-cies exist between AoA trends computed from observations, models and reanalyses (Garny et al., 2024b). In Chabrillat et al. (2018), the difference in absolute AoA between the CTM driven by different reanalyses is at most 1 year in the tropical lower stratosphere and up to 2 years or more in the upper stratosphere, with trends over 2002–2015 rang-ing from -0.4 to 0.4 years per decade above 10 hPa. Chem-istry climate models suggest decreasing stratospheric age of air trends around 0.1–0.2 years per decade. Balloon observa-tions, on the other hand, show positive trends on the order of 0.1–0.3 years per decade (Garny et al., 2024b). The cause of these discrepancies is not clear.

In this work, the implementation of SF$_6$ in the Belgian Assimilation System for Chemical ObsErvations (BASCOE) chemistry transport model (CTM) is described. The imple-mentation of SF$_6$ is evaluated using independent satellite ob-servations from MIPAS (Michelson Interferometer for Pas-sive Atmospheric Sounding, Fischer et al., 2008) and ACE-FTS (Atmospheric Chemistry Experiment Fourier Transform Spectrometer, Bernath et al., 2005), and via the computation of the global atmospheric lifetime of SF$_6$, which is compared with the literature. Three recent meteorological reanalyses have been used to drive the BASCOE simulations: ERA5 (ECMWF Reanalysis V5, Hersbach et al., 2020), MERRA2 (Modern-Era Retrospective analysis for Research and Ap-plications V2, Gelaro et al., 2017) and JRA-3Q (Japanese Reanalysis for Three Quarters of a Century, Kosaka et al., 2024). These reanalyses extend upwards to 0.01 hPa in the mesosphere where SF$_6$ chemistry is important. In this study we use three different sets of reanalysis data to drive the BASCOE model in order to analyse the influence of the me-teorology on the results. Due to a large spread of the life-time values, both those presented here as well as those found in the literature, the work was extended to five other long-lived species to support the evaluation of our methods and re-sults: N$_2$O, CH$_4$, CFC-11, CFC-12 and HCFC-22. These six species can be used to compute the AoA using the method from Voet et al. (2025). However, AoA diagnostics are not presented in this work.

The paper is organised as follows: Section 2 introduces the different data sets used. This includes MIPAS and ACE-FTS observations and the three reanalyses. Section 3 dis-cusses the BASCOE model simulations, and in particular the implementation of the chemistry of SF$_6$ and the set-up of the model. Section 4 describes the computation of the global atmospheric lifetime. Finally, the comparison between the model simulations and the observations is presented in Sect. 5, along with the obtained values for the global lifetime. The conclusions are presented in Sect. 6. While this study compares diagnostics of the reanalyses, it does not present a full inter-comparison of the reanalyses themselves.

2 Data sets

The following sections describe the data sets that are used in this work. The first two subsections deal with the satellite data that are used to evaluate the model results. The last sub-section informs about the reanalysis data sets that are used as input for the BASCOE CTM. We used two satellite data sets as observational reference, namely MIPAS and ACE-FTS. These are described in more detail below. As drivers for BASCOE, three different reanalyses were used, namely ERA5, MERRA2, and JRA-3Q. Details about these reanaly-ses are given below.

2.1 MIPAS

The Michelson Interferometer for Passive Atmospheric Sounding (MIPAS, Fischer et al., 2008), onboard the EN-VISAT satellite, operated from July 2002 until April 2012 in a sun-synchronous low-Earth orbit. It is a Fourier Transform Spectrometer with a limb viewing geometry, measuring atmospheric infrared radiation from which vertical profiles of trace gases are retrieved. MIPAS was designed to measure over 20 species, including SF$_6$, CFC-11 and CFC-12, CH$_4$, N$_2$O and HCFC-22. In April 2004, MIPAS had a failure and observations were halted until January 2005, after which measurements resumed with reduced spectral resolution. MIPAS datasets are thus typically split into two phases: one with high spectral resolution and one with reduced spectral resolution. In this study, the model output is evaluated using MIPAS V8 data from the IMK/IAA research processor, developed by the Institut für Meteorologie und Klimaforschung (IMK) and the Instituto de Astrofísica de Andalucía (IAA) (MIPAS, 2019). To judge the model differences with respect to MIPAS and ACE-FTS observations, we compare with typical instrumental differences from satellite validation studies. These validation studies are summarized in Table 1 with their data versions. Most of the instrument differences between ACE-FTS and MIPAS are between 10 % and 20 %, particularly for the species CH$_4$, N$_2$O and CFC-12. However, the agreement depends on the altitude and differences increase significantly above 50 hPa for some species.

2.2 ACE-FTS

The Atmospheric Chemistry Experiment Fourier Transform Spectrometer (ACE-FTS) is a Canadian-led mission on SCISAT-1 (Bernath et al., 2005). It started taking measurements in February 2004 and is still operational after more than 20 years on orbit. This instrument performs infrared solar-occultation measurements on an inclined circular orbit. ACE-FTS takes measurements twice per orbit, during sunrise and sunset, allowing for up to 30 observations per day. ACE-FTS focuses on the region in the stratosphere that contains the ozone layer and measures 70 atmospheric trace gases, including CFC-11, CFC-12, CH$_4$, N$_2$O and HCFC-22. The data version used in this work is V5.3 (ACE-FTS, 2025).

2.3 Reanalyses

Three different reanalysis data sets are used to drive the BAS-COE chemistry transport model. Reanalyses offer a globally complete data set of atmospheric variables by assimilating observational data into models to ensure spatial and temporal homogeneity. Reanalyses with a top around 0.01 hPa were chosen to capture mesospheric circulation features that are important for the chemistry of SF$_6$.

The first reanalysis is the ERA5 (Hersbach et al., 2020) data set, issued by the European Centre for Medium-Range Weather Forecasts (ECMWF). It is available from 1940 onwards. The ERA5 atmospheric data has a horizontal resolution of 31 km ($\sim 0.28125°$), and 137 vertical levels from the surface up to 0.01 hPa.

Similarly, the Modern-Era Retrospective analysis for Research and Applications version 2, or (MERRA2, Gelaro et al., 2017), is a data set from the Global Modelling and Assimilation Office (GMAO) which covers the period 1980 to present. The data set has a horizontal resolution of $0.5° \times 0.625°$ and 72 vertical levels, from the surface up to 0.015 hPa. MERRA2 is the only one of the three reanalysis data sets used here that assimilates Aura Microwave Limb Sounder (Aura MLS) temperature profiles from 2004 onwards above 5 hPa (SPARC, 2022).

Finally, the Japanese Reanalysis for Three Quarters of a Century (JRA-3Q, Kosaka et al., 2024) is the third long-term reanalysis produced by the Japan Meteorological Agency (JMA), covering the period from September 1947 to present. This is the most recently released data set of the three reanalyses used in this work. JRA-3Q has a higher resolution than its predecessor JRA-55: it has a horizontal resolution of 40 km ($\sim 0.359°$) and 100 vertical levels from the surface to 0.01 hPa.

Each reanalysis has a sponge layer at the model top to avoid unphysical reflection of wave energy at a rigid model lid. These sponge layers are implemented differently in each reanalysis and can explain some of the differences found at the upper levels and in our results. According to SPARC (2022, Chap. 5) the climatological wave driving and the climatological circulation strength and structure agree closely among the most recent reanalysis products available at the time (MERRA2, ERA5 and JRA-55), however, MERRA2 is shown to have slower upwelling in the tropics than the other reanalyses. This slower BDC is confirmed by tracer-transport studies, indicating that the difference is not only related to the radiation budget, but also to transport (SPARC, 2022, Chap. 5). The SPARC report advises to use MERRA2 with caution in Brewer–Dobson circulation studies and for many BDC diagnostics, JRA-55 and ERA-Interim are more suitable (with limitations). Ploeger et al. (2021) showed that ERA5 has a slow circulation compared to ERA-Interim and found similarities between ERA5 and MERRA2 in the tropical upwelling and the evolution of the residual circulation transit times. ERA-Interim and JRA-55 are not used here because these do not reach high enough to capture the mesospheric chemistry of SF$_6$.

3 The BASCOE model

The model that is used in this work is the Chemistry Transport Model (CTM) of the Belgian Assimilation System for Chemical ObsErvations (BASCOE, Errera et al., 2008). This CTM is dedicated to stratospheric composition and includes around 60 chemical species. All species are advected by the

Table 1. Summary of observational differences between ACE-FTS and MIPAS from validation studies. The data versions used in this work are MIPAS IMK/IAA V8 and ACE-FTS V5.3.

Species	Validation study	Data versions	Agreement
SF$_6$	SPARC (2017)	ACE-FTS V2.2, MIPAS spectral version 5	$\pm 2.5\%$ difference with multi-instrument mean below 50 hPa for annual mean profiles. Above 50 hPa, mostly within $\pm 5\%$, some regions $\pm 10\%$ to $\pm 20\%$. Monthly mean profiles generally consistent, with slightly larger deviations for some months.
N$_2$O	Sheese et al. (2017)	ACE-FTS V3.5, MIPAS spectral version 5, MLS V3.3	ACE-FTS shows -9% to $+7\%$ differences with MIPAS and -21% to 5% with MLS below 35 km. Above 35 km, agreement within $\pm 10\%$.
CFC-11	SPARC (2017)	ACE-FTS V2.2, MIPAS spectral version 5	MIPAS monthly mean profiles show 5%–10% difference with ACE-FTS below 100 hPa. ACE-FTS shows up to 50% difference to multi-instrument mean at 30 hPa.
CFC-12	SPARC (2017)	ACE-FTS V2.2, MIPAS spectral version 5	Differences between monthly mean profiles within $\pm 10\%$ across the vertical range.
CH$_4$	Laeng et al. (2015)	ACE-FTS V3.5, MIPAS spectral version 5	12% difference between 20 and 65 km. Difference of 15% at 17 km.
	SPARC (2017)	ACE-FTS V2.2, HALOE V19, MIPAS spectral version 5	Differences of between the monthly mean profiles of up to $\pm 20\%$ to the multi-instrument mean.
HCFC-22	Kolonjari et al. (2024)	ACE-FTS V5.2, MIPAS IMK/IAA V8	$+3\%$ to 10% difference between 5 and 10 km. $\pm 5\%$ difference between 10 and 21 km. $+5\%$ to 14% difference between 21 and 25 km.

flux-form semi-Lagrangian scheme (Lin and Rood, 1996) which conserves mass and preserves tracer-tracer correlations. Approximately 200 chemical reactions (gas phase, photolysis and heterogeneous) are taken into account, including a parametrization of Polar Stratospheric Cloud (PSC) microphysics (Errera et al., 2019). The gas-phase and photolysis reaction rates have been updated according to Burkholder et al. (2015). Chemical reactions are solved by a chemical kinetic preprocessor (KPP, Damian et al., 2002). Note that chemistry is not computed in the troposphere at altitudes below 400 hPa. The CTM is driven by meteorological analyses as described in Sect. 3.2. The following subsections first describe the update of the chemistry and then the preprocessing of the dynamical fields and details of the simulations.

3.1   Implementation of SF6 chemistry

SF$_6$ is inert in the stratosphere and is destroyed by attachment of electrons in the mesosphere producing a negative excited ion (SF$_6^-$)*. SF$_6$ is partially recovered via stabilizing reactions, either directly via photodetachment of an electron, or by cycling the stabilized SF$_6^-$ back to SF$_6$ via several other reactions.

In order to model the distribution of SF$_6$, the BASCOE chemistry transport model has been updated with SF$_6$ chemistry. The reaction scheme used in this work was first de-

scribed in Reddmann et al. (2001) and later used in the EMAC model (Loeffel et al., 2022). It is shown in Table 2. The main destruction mechanism for SF$_6$ is auto-attachment of electrons (Reaction R2). UV-photolysis (Reaction R1) is not used in BASCOE because the corresponding loss rate is negligible compared to the loss rate from electron auto-attachment (Totterdill et al., 2015). In addition to SF$_6$, the species SF$_6^-$ and (SF$_6^-$)* have been added to the list of chemical compounds of BASCOE and the rate constants for the reactions were taken from Reddmann et al. (2001). We only consider the fast electron-attachment reaction and neglect the destructive branch, which accounts for less than 0.1% of the total reaction (Miller et al., 1994). The fast electron-attachment reaction produces an excited negative ion of SF$_6$, which in turn can stabilize and react with H, HCl, O3 or $h\nu$ to form SF$_6$ or other products. In order to implement these chemical reactions, the electron density and the computation of the photodetachment rate are needed. The electron density is parametrized taking as input the altitude, the latitude, the solar zenith angle, the O$_2$ column, the air density and the day of the year, using the same code as in EMAC (Reddmann et al., 2001; Loeffel et al., 2022). The relevant electrons are those from the D-region of the ionosphere (see Brasseur and Solomon, 2005, Chap. 7, for a derivation of the electron density), which is located roughly between 60

and 90–95 km, and thus lies mostly within the mesosphere. The electron density assumes mean solar activity.

We use an electron-attachment rate that is specific for thermalized electrons ($\ll 1$ eV), resulting in fast attachment. As thermalization is fast at the altitudes relevant for electron-attachment, the use of the full electron density is justified. The photodetachment (Reaction R3) rate is calculated within the BASCOE model as a standard photolysis rate, via:

$$j_3(\theta) = \sum_i \sigma_{pd}(\lambda_i) F(\theta, \lambda_i, p) \Delta\lambda_i \qquad (1)$$

Where σ_{pd} is the cross-section for photodetachment and F is the solar irradiance (actinic flux), dependent on the solar zenith angle θ, the wavelength λ_i and the pressure p. The cross-sections σ_{pd} are computed using a relation proposed by Datskos et al. (1995) for wavelengths below 337 nm and a constant cross-section of 2×10^{-18} for wavelengths above 337 nm, as proposed by Ingólfsson et al. (1994). The cross-sections as a function of wavelength and the photodetachment rate for one snapshot of BASCOE output as a function of latitude and corresponding solar zenith angle are shown in Fig. 1.

The loss rates α and the electron density computed in BASCOE were evaluated against published values. Figure 2a shows how the inverse loss rates from Reddmann et al. (2001) compare to the inverse loss rates in BASCOE on 15 January 2002. This plot also contains the loss rates from Totterdill et al. (2015), which agree well with the loss rates in BASCOE. The electron density in BASCOE is compared with other published electron fields in Fig. 2b. This shows that BASCOE follows the ionization profile from Reddmann et al. (2001). BASCOE electron density also agrees well with an observation taken from Brasseur and Solomon (2005), shown in Fig. 2b.

3.2 Model simulations

This work presents three BASCOE CTM simulations of 25 years (1997–2023) driven by ERA5, MERRA2 and JRA-3Q, respectively, with a model time step of 30 min (see Table 3 summarizing the BASCOE simulations performed for this study). Reanalysis dynamical fields were reduced in resolution to match the BASCOE spatial grid using a mass-conserving preprocessor, following the approach in Chabrillat et al. (2018). This was done because simulating chemistry on the native spatial grids of the reanalyses incurs a large computational cost and storage requirements which are not available on the BIRA-IASB computing system. The BAS-COE simulations have been carried out with a horizontal resolution of $2° \times 2.5°$ latitude-longitude as in Chabrillat et al. (2018), which is sufficient to capture tropical and high-latitude mixing barriers (Strahan and Polansky, 2006). Similarly, the vertical resolution of the reanalyses has been reduced, since chemistry is not computed on most levels in the troposphere. The vertical regridding procedure is detailed in

Appendix A. The native vertical resolution of the reanalyses and those obtained by the vertical regridding are shown in Fig. 3. For ERA5, a grid with 61 levels was chosen, for MERRA2, 49 levels were chosen and finally the grid of JRA-3Q was reduced to 53 levels. From this figure it is clear that the resolution is now lower in the troposphere, thus removing unnecessary levels, while also being somewhat reduced in the stratosphere and mesosphere.

To assess the transport on the reduced vertical grids, simulations of mean AoA using an idealized clock tracer were performed on both the native and the reduced grids. These simulations re-use meteorological fields from the same two years (1980–1981) of reanalysis data to drive the model in order to avoid the effect of climatological trends. Two years were chosen instead of one to capture the dynamical effects of the Quasi Biennial Oscillation (QBO), which is called a perpetual QBO set-up (Prignon, 2021). Each run lasts 20 years and the results are evaluated at the end of this period to avoid the spin-up of the model. The average of the model AoA from the last year of the perpetual QBO simulations is shown in Fig. 4. MERRA2 meteorology results in the highest AoA, followed by JRA-3Q, while ERA5 produces the lowest AoA. This could indicate a faster circulation with ERA5 compared to MERRA2 and JRA-3Q in the BASCOE model. The simulations on the reduced and native grids are in good agreement, generally within 0.1 years. Slightly larger differences are found for MERRA2 (0.3 years) in the extra-tropics at 100 hPa, which is acceptable. This validates our choice for the reduced levels.

Initial conditions were based on a BASCOE run driven by ERA5 (see Prignon et al., 2021), except for SF$_6$. For the latter, monthly zonal mean output from an EMAC model simulation was used to initialize the BASCOE simulations on 27 January 1997. This output comes from the specified dynamics simulation described in Loeffel et al. (2022), which has a model top at 0.01 hPa, spans the period 1980–2011 and is nudged to the ERA-Interim reanalysis. The lower boundary conditions for BASCOE were adapted from Meinshausen et al. (2017) for surface emissions from 1700 to 2014, and from Gidden et al. (2019) for emission projections under the shared socioeconomic pathway SSP2-4.5 beyond 2014.

At every time step of the simulation, BASCOE checks if observations are available for that time and interpolates the model output at the locations of the satellite observations. BASCOE was initially saved on the spatial grid of MIPAS V5 and ACE-FTS V4.1. Although newer data versions were later used, the model output was not re-interpolated to the new data locations, and therefore only subsets of the new data are used. This output in observation space is used to compute statistical differences between the model and the observations, presented in Sect. 5.1.

Table 2. Chemical scheme for SF_6. The reaction in bold is not included.

Reaction No.	Reaction	Reaction rate constant	Remarks
R1	**$SF_6 + h\nu \rightarrow$ products**		**UV-photolysis**
R2	$SF_6 + e^- \rightarrow (SF_6^-)^*$	$k_2 = 270 \times 10^{-9}\,\mathrm{cm^{-3}\,s^{-1}}$	e^- auto-attachment
R3	$SF_6^- + h\nu \rightarrow SF_6 + e^-$	$j_3 \approx 0.02\,\mathrm{s^{-1}}$	photodetachment[1]
R4	$SF_6^- + H \rightarrow SF_5^+ + HF$	$k_4 = 0.21 \times 10^{-9}\,\mathrm{cm^{-3}\,s^{-1}}$	
R5	$(SF_6^-)^* + M \rightarrow SF_6^-$	$k_5 = 0.19 \times 10^{-9}\,\mathrm{cm^{-3}\,s^{-1}}$	stabilization
R6	$(SF_6^-)^* \rightarrow SF_6 + e^-$	$k_6 = 1 \times 10^6\,\mathrm{s^{-1}}$	auto-detachment[2]
R7	$SF_6^- + HCl \rightarrow$ products	$k_7 = 1.5 \times 10^{-9}\,\mathrm{cm^{-3}\,s^{-1}}$	
R8	$SF_6^- + O_3 \rightarrow SF_6 + O_3^-$	$k_8 = 1.2 \times 10^{-9}\,\mathrm{cm^{-3}\,s^{-1}}$	

[1] The value of j_3 is an indication of the final result of the photodetachment calculation.
[2] There is a typo in Table 1 of Reddmann et al. (2001) and the correct value was taken from its Sect. 2.2.
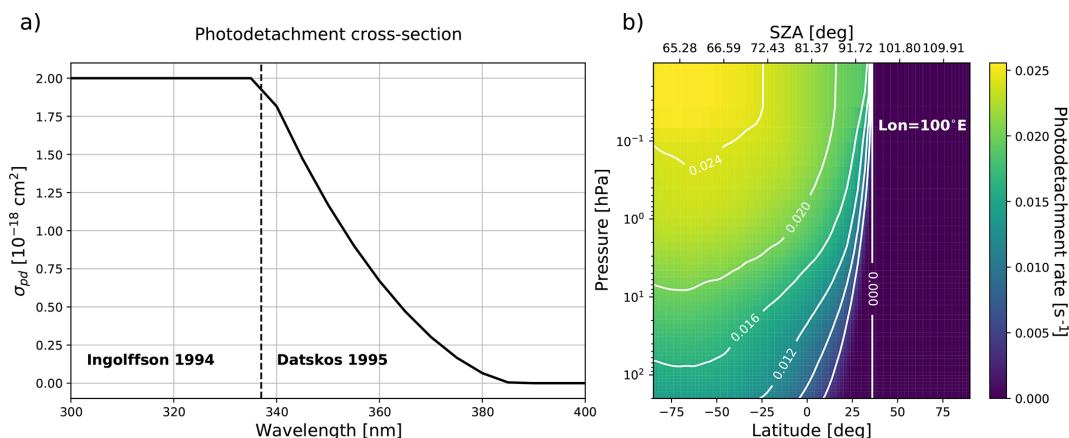

Figure 1. Left: photodetachment cross-sections computed from Ingólfsson et al. (1994) and Datskos et al. (1995). Right: photodetachment rate, computed in BASCOE, as a function of latitude with corresponding solar zenith angle (SZA) for a longitude of 100° E on 1 January 2002 at 00:00 UTC.

4 Global atmospheric lifetime

While evaluation of the model results with satellite observations is useful, it only provides validation for altitudes seen by the instruments. The global atmospheric lifetime of a gas, on the other hand, probes the entire atmosphere and can thus be used as a diagnostic for the implementation of the SF_6 chemistry, as well as for the reanalysis data sets used in this work, by assessing the differences between the three simulations. The global atmospheric lifetime of species i is calculated at any time from BASCOE model output as the ratio between the global atmospheric burden and the global atmospheric loss rate:

$$\tau = \frac{\text{atmospheric burden}}{\text{atmospheric loss rate}} \quad (2)$$

which can be found in, for example, the 2013 SPARC report on lifetimes, Chap. 2 (SPARC, 2013). This is the instantaneous lifetime and depends on the specific atmospheric conditions. The atmospheric burden is calculated as the total number of molecules of the species i, in other words

$\int n_i \mathrm{d}V = \int \chi_i n_{\text{air}} \mathrm{d}V$ where n_i is the number density of species i, n_{air} is the air density, χ_i is the volume mixing ratio of species i, and the integral runs over all grid cells of the model with volume $\mathrm{d}V$. The atmospheric loss rate is a similar integral, but it includes the net chemical loss frequencies α_i, so that the integral is given by $\int \alpha_i n_i \mathrm{d}V$. The loss rate of species i is written as:

$$\frac{\mathrm{d}n_i}{\mathrm{d}t} = -\alpha_i n_i \quad (3)$$

with

$$\alpha_i = L_i - \frac{P_i}{n_i} \quad (4)$$

where P_i is the local production of species i in $\mathrm{molec\,cm^{-3}\,s^{-1}}$, and L_i is the local loss in $\mathrm{s^{-1}}$. These quantities P_i and L_i are computed by the chemical kinetic preprocessor and stored in the output files of BASCOE. Using Eqs. (3) and (4) the global lifetime can be computed from every snapshot of model output. To smooth out seasonal variability, the lifetime is averaged over the period 2002–2012. This is an instantaneous lifetime, which can differ from
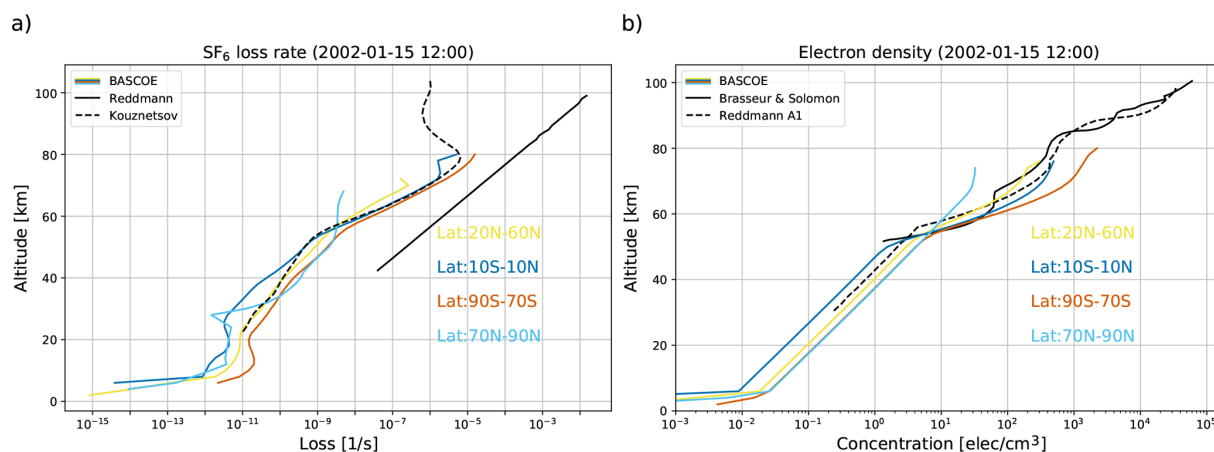
a)

b)

Figure 2. Left: comparison between the loss rates as shown in Reddmann et al. (2001) and Totterdill et al. (2015) with a BASCOE snapshot from 15 January 2002 (TRANS_M2_L49) in different latitude bands. Right: example profiles of the electron field of BASCOE, shown over 4 latitude bands, compared with the A and A1 profiles of Reddmann et al. (2001) and the electron density in Brasseur and Solomon (2005), Chap. 7, Fig. 7.3.

Table 3. BASCOE runs performed in this study.

Label	Description	Simulated period	Chemistry
TS_E5_L137	Time slice simulation (perpetual QBO) driven by ERA5 on native grid	20 years	no
TS_E5_L61	Time slice simulation (perpetual QBO) driven by ERA5 on reduced grid with 61 levels	20 years	no
TS_M2_L72	Time slice simulation (perpetual QBO) driven by MERRA2 on native grid	20 years	no
TS_M2_L49	Time slice simulation (perpetual QBO) driven by MERRA2 on reduced grid with 49 levels	20 years	no
TS_J3Q_L100	Time slice simulation (perpetual QBO) driven by JRA-3Q on native grid with 100 levels	20 years	no
TS_J3Q_L53	Time slice simulation (perpetual QBO) driven by JRA-3Q on reduced grid with 53 levels	20 years	no
TRANS_E5_L61	Transient simulation driven by ERA5 on 61 levels	1997/01–2023/12	yes
TRANS_M2_L49	Transient simulation driven by MERRA2 on 49 levels	1997/01–2023/12	yes
TRANS_J3Q_L53	Transient simulation driven by JRA-3Q on 53 levels	1997/01–2023/12	yes

the steady-state lifetime that is computed under equilibrium conditions, where the sinks and sources of the gas are balanced such that the burden remains constant. This condition is only fulfilled in specific simulations with constant reactant species. Other methods exist to compute the atmospheric lifetime from observations. See, for example, Plumb and Ko (1992), who developed a method to relate lifetimes of two species to the slope of the linear relation between the mixing ratios of two species in gradient equilibrium. The advantage of this method is that this can be done with observations of the extratropical lower stratosphere, but the drawback is that the lifetime of one of the two species must be known to derive a relative lifetime for the other one. In contrast, the bur-

den divided by the loss, computed from model output, yields an absolute lifetime, but a limitation is that the uncertainties on the loss processes in models can be difficult to assess.

In the following, the lifetime is computed from model output for the six long-lived trace gases: SF$_6$, N$_2$O, CH$_4$, CFC-11, CFC-12 and HCFC-22. For CH$_4$ and HCFC-22, reaction with OH in the troposphere is the most important destruction process. Since BASCOE does not compute chemistry in the lower troposphere, only the stratospheric lifetime (and not the global lifetime) of these species is computed, i.e., integrating the loss rates above 200 hPa in the tropics (between ±30°) and above 400 hPa at other latitudes. The oceanic absorption of N$_2$O is not taken into account in this work. This
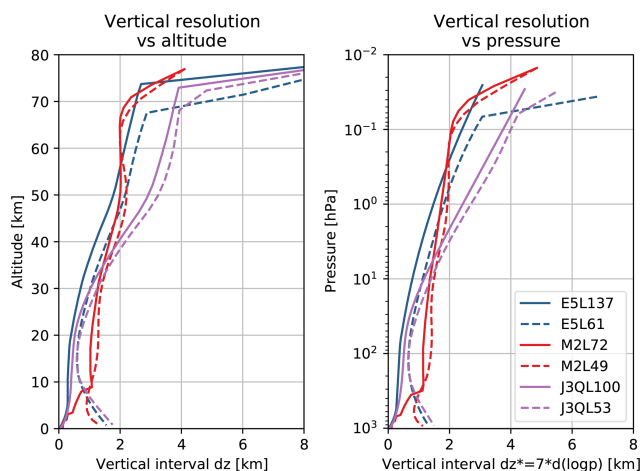
Figure 3. Vertical resolution of the different grids as a function of altitude (left) and the pressure (right). Blue, red and purple lines correspond, respectively, to ERA5, MERRA2 and JRA-3Q. Solid and dashed lines correspond, respectively, to native and reduced vertical resolution. Note that the line color of each reanalysis follows the A-RIP conventions, as in other figures.
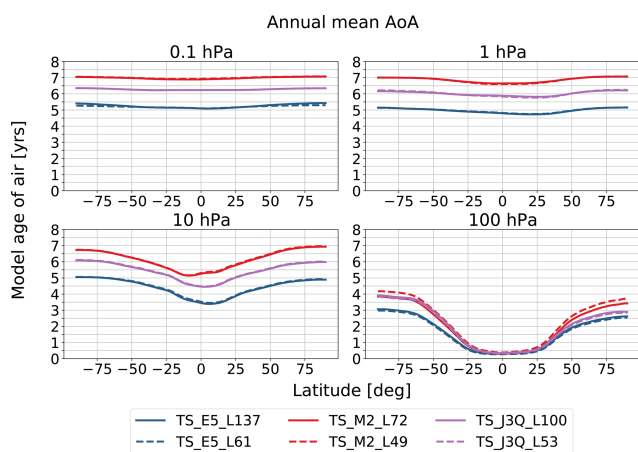

Figure 4. Model age of air from perpetual QBO simulations driven by ERA5, MERRA2 or JRA-3Q on their native (solid lines) and reduced (dashed lines) vertical grids, at different altitudes, averaged over the last year of the simulation.

oceanic sink of atmospheric N$_2$O is often overlooked. It is described as modest, but significant (de la Paz et al., 2025).

5 Results and discussion

5.1 Comparison with independent observations

The results of the BASCOE simulations have been compared to MIPAS and ACE-FTS satellite observations. The normalized mean difference (NMD) between the BASCOE simulation and the satellite profiles, computed as observation minus model divided by the model, the associated standard devia-

tion (STD) and their correlations (Correl) are shown in Fig. 5 in the tropics and in Fig. 6 in the southern high latitudes (60–90° S). These statistics are computed over the period January 2005–April 2012 for MIPAS and February 2004–April 2012 for ACE-FTS. The grey shading indicates differences between MIPAS and ACE-FTS as discussed in Table 1. For CH$_4$ we used a conservative value of ±20 %. For SF$_6$, the agreement between the BASCOE model runs and MIPAS is mostly within the instrument differences for MERRA2 and JRA-3Q, with ERA5 at the edge of the grey envelope. Agreement with ACE-FTS is within the uncertainties between 100 and 20 hPa. The differences with both instruments are limited to approximately ±10 %. Note that instrument differences between ACE-FTS and MIPAS can reach up to ±10 % to ±20 % in certain regions, but this was not included in the envelope.

For N$_2$O slightly larger differences are found between 10 and 50 hPa, but agreement is in line with instrumental differences below 50 hPa. For CH$_4$, the comparisons are within the range of uncertainty between MIPAS and ACE-FTS below 10 hPa and increase at high altitude where the chemical losses are more pronounced. For CFC-11 in the lower stratosphere, the difference is also in agreement with the instrumental differences and for HCFC-22 the difference is in agreement with the instrumental differences of around 14 % at 25 km (∼ 25 hPa) found in Kolonjari et al. (2024). For CFC-12 the differences with ACE-FTS are somewhat larger than expected, showing differences of more than 20 % above 30 hPa, which is larger than the 10 % instrumental differences between MIPAS and ACE-FTS (SPARC, 2017). An explicit comparison between MIPAS and ACE-FTS is difficult here due to their different sampling. For SF$_6$ the simulation driven by MERRA2 shows smaller differences with respect to MIPAS than the simulations driven by ERA5 or JRA-3Q. For all species, the standard deviation is relatively small (< 10%) at altitudes where their photochemical loss is small and increases at higher altitude. The correlation is also better in the lower stratosphere (> 0.8) and decreases at higher altitude.

Figures 7 and 8 show time series of the normalized mean difference (NMD) and the normalized standard deviation (NSD) at different levels for SF$_6$. The time series in Fig. 7 emphasizes the temporal stability of the results in the tropics and at mid to low altitude. The difference is relatively stable and limited mostly to 10 % in the tropics. At the Poles, the differences show seasonal variability with an amplitude around 20 % at 1 hPa. The seasonality of the differences are also reflected in the standard deviation.

This oscillating pattern is found for all trace gases in this study (see the Supplement where similar figures for the other long-lived tracers are available). The standard deviation is around 10 %–15 % in the tropical lower stratosphere and increases towards the Poles.

The standard deviation shows a slight decreasing trend. This is due to the fact that the surface emissions of SF$_6$ sig-
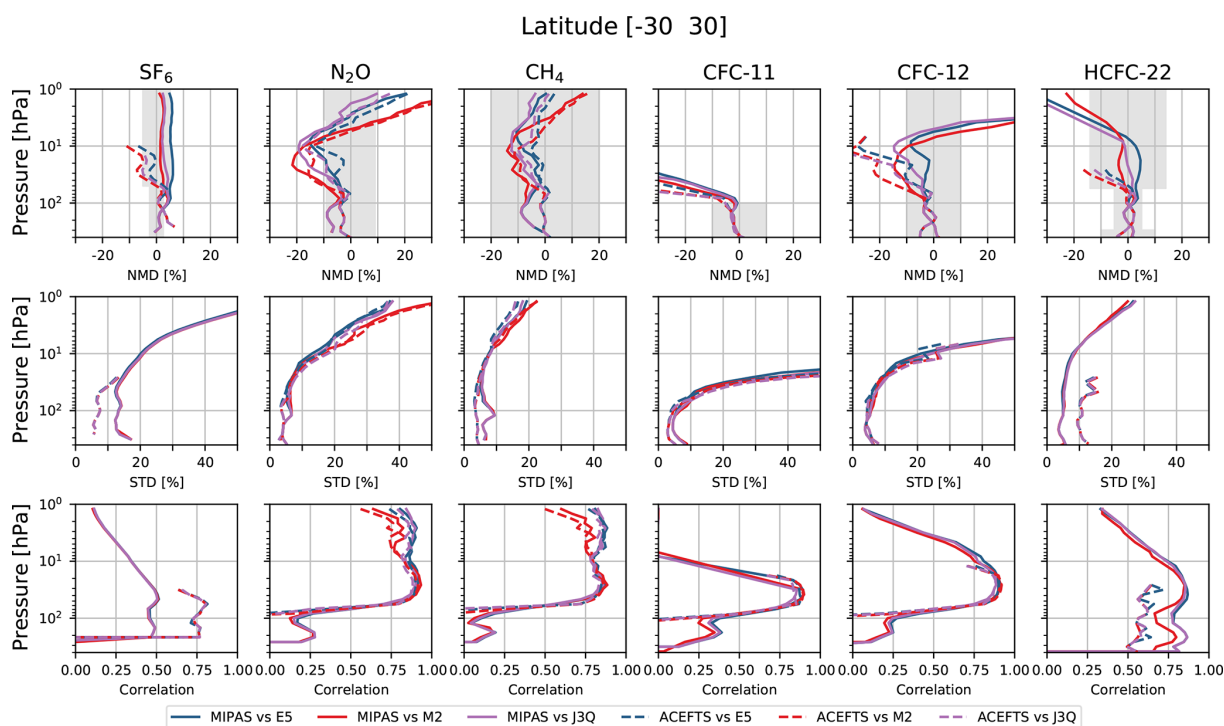
Figure 5. Normalized mean difference (observation-model)/model (NMD), standard deviation (STD) and correlation (Correl) of all six long-lived species over the tropics. Data is cut off at 1 hPa because there are insufficient observations above this pressure level. The grey shading indicates typical differences between MIPAS and ACE-FTS.
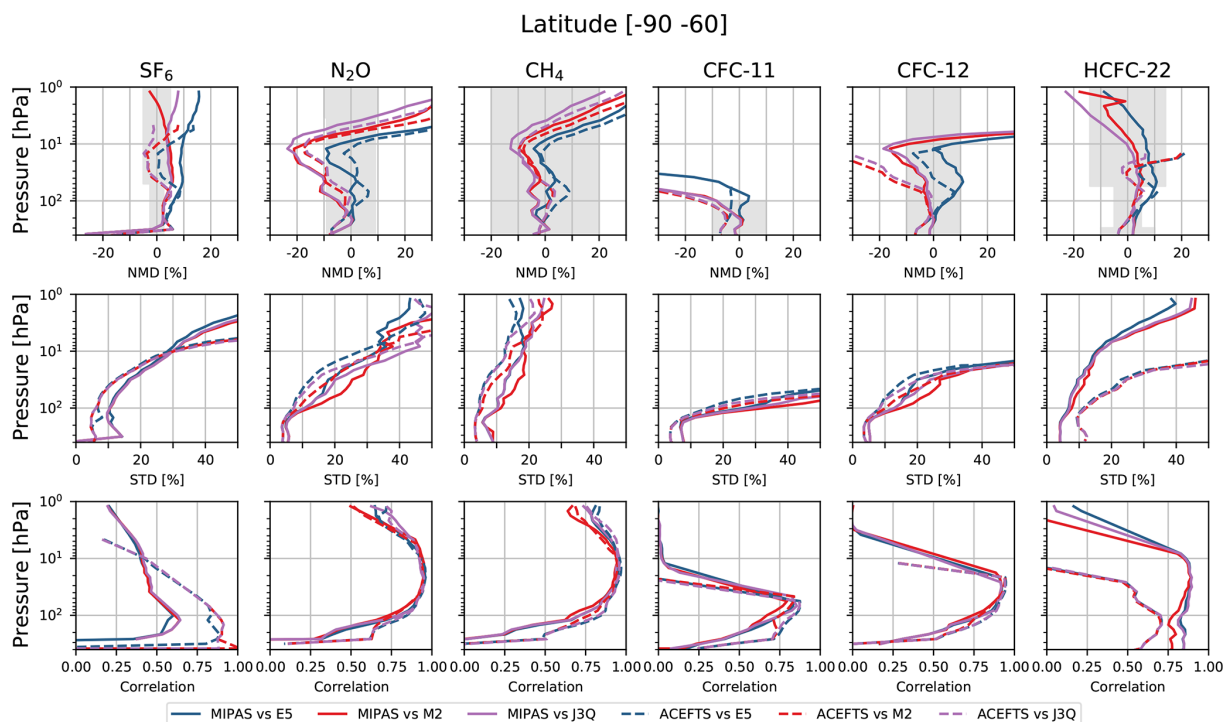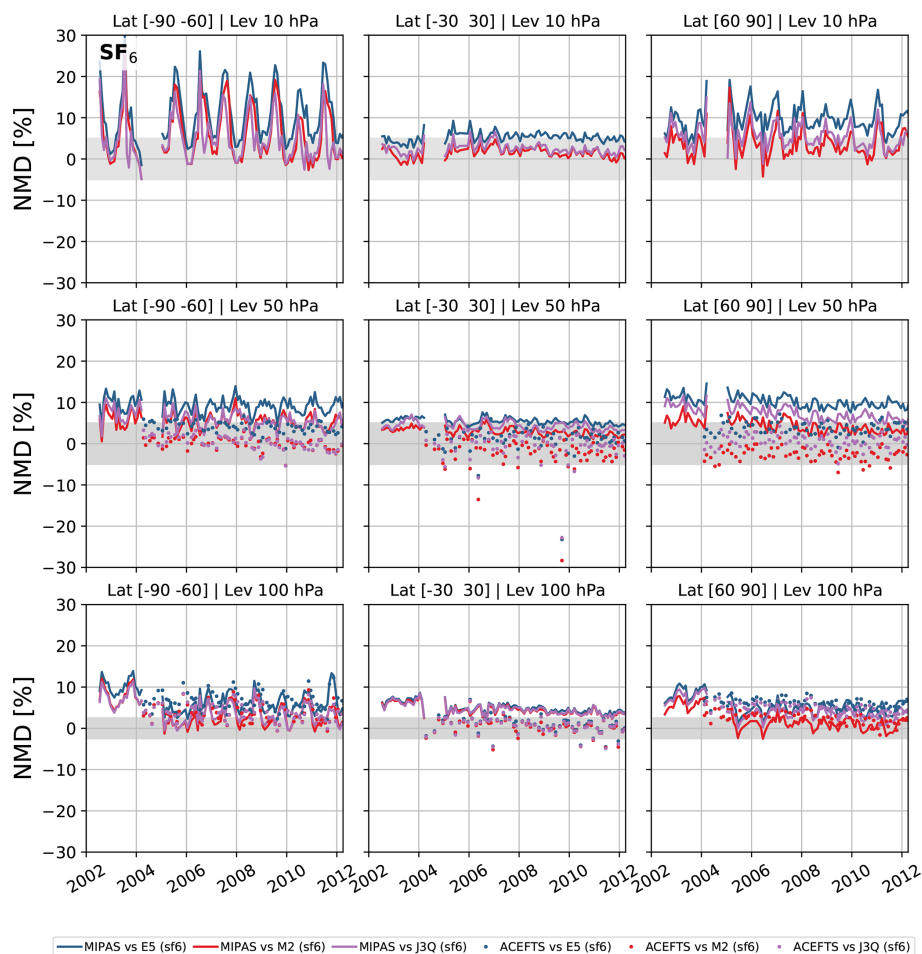

Figure 6. Same as Fig. 5, but for the South Pole.

Figure 7. Timeseries of the normalized mean difference of SF$_6$ volume mixing ratios with respect to MIPAS and ACE-FTS for three latitude bands and three pressure levels. Grey shading indicates the uncertainties between MIPAS and ACE-FTS from validation studies.

nificantly increase over the course of the shown period, thus reducing the relative noise in the observations. A similar pattern is found for HCFC-22 for the same reason (see Fig. S16 in the Supplement).

5.2   Global atmospheric lifetime

Figure 9 shows the global atmospheric lifetimes from the three BASCOE runs and the multi-reanalysis mean (MRM), averaged over 2002–2012. The error bars indicate the 1σ variability of the lifetime time series from BASCOE over the considered period 2002–2012. The results are compared with lifetimes found in the literature, shown as error bars here to indicate the possible range of values with a marker at the best value if provided in the source paper. Note that these reference values are not specifically for the period 2002–2012 and that the error bars represent different quantities and are not actual uncertainties. Note also that some lifetime estimates are model based, while other lifetimes are derived from observations. Model based lifetime estimates usually rely on

the assumption of a steady-state atmosphere. Minschwaner et al. (2013) computed a correction factor for transient lifetimes of CFC-11 and CFC-12 and showed that the difference between transient and steady-state lifetimes was on the order of 1 %–2 % for these species. This correction factor takes into account the time it takes for tropospheric increases or decreases to propagate to the loss region in the stratosphere. The lifetimes of the long-lived species N$_2$O, CH$_4$, CFC-11, CFC-12 and HCFC-22 (see Fig. 9a) show good agreement with results from the literature (SPARC, 2013; Volk et al., 1997; Prather et al., 2023; Fleming et al., 2015; Minschwaner et al., 2013; Moore and Remedios, 2008; Avallone and Prather, 1997; Kanakidou et al., 1995; Spivakovsky et al., 2000) and between the reanalyses. For CH$_4$ and HCFC-22, only stratospheric lifetimes are shown. Note that none of the N$_2$O lifetimes presented here take into account the uptake by oceans. We hypothesize that the true lifetime of N$_2$O is thus smaller than what is found here. Our lifetime of CH$_4$ is remarkably higher than that of Volk et al. (1997), which could be due to uncertainties in the OH concentrations. We
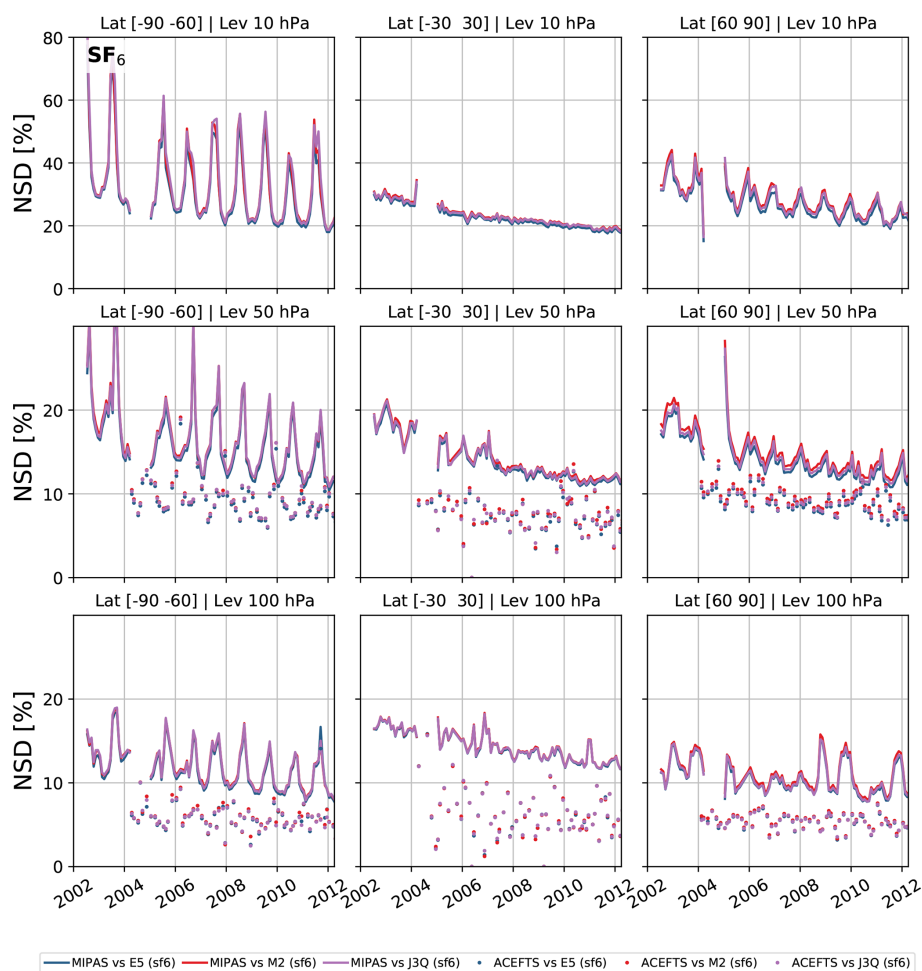
Figure 8. Timeseries of the standard deviation of SF6 for three latitude bands and three pressure levels.

also find a lower HCFC-22 lifetime than Moore and Remedios (2008), which may similarly reflect differences in modelled OH concentrations.

The consistency between the three different simulations for the 5 species mentioned above and the agreement with the literature creates confidence in our lifetime computation. While these species have much shorter lifetimes than SF6 and have sinks in different regions, the diagnostic used here is independent of the absolute lifetime for species with well-defined loss processes. A limitation of the validation of the lifetime computation is that losses outside of the model domain are not taken into account. However, BASCOE reaches altitudes of around 80 km where the maximum loss of SF6 occurs (Kouznetsov et al., 2020). The lifetimes of all six species are summarized in Table 4. The global atmospheric lifetime of SF6 has been computed in several studies over the last 30 years (Krey et al., 1977; Ravishankara et al., 1993; Ko et al., 1993; Morris et al., 1995; Harnisch et al., 1999; Reddmann et al., 2001; Patra et al., 1997; Ray et al., 2017; Kovács et al., 2017; Kouznetsov et al., 2020; Loeffel et al., 2022). This body of work is summarized in Fig. 9b. The black

bars are organized (from left to right) from the oldest to the most recent publication. Some of these estimates were derived from models, while others were derived from observations so that this panel does not represent an evolution in model development. Despite the number of estimates, the atmospheric lifetimes show a large spread. Ravishankara et al. (1993) obtained a lifetime of 3200 years from model computations considering only UV-photolysis and a slow electron attachment that leads to destruction of SF6. The lower limit mentioned there was obtained by maximizing removal by combustion. Later modelling studies like Morris et al. (1995) reduce the lifetime of SF6 from 3200 years to around 800 years by considering also a fast, non-destructive electron attachment branch. In the present study, the average lifetime of SF6 in BASCOE over the period 2002–2012 is 2646 ± 532 (1σ) years with an ERA5 driven run, 1909 ± 182 (1σ) years with a MERRA2 driven run and 2145 ± 459 (1σ) years with a JRA-3Q driven run. The uncertainty on the lifetime coming from the choice of reanalysis can also be estimated as the root of the squared differences with respect to the MRM. This yields an uncertainty of 532 years, similar to the standard de-
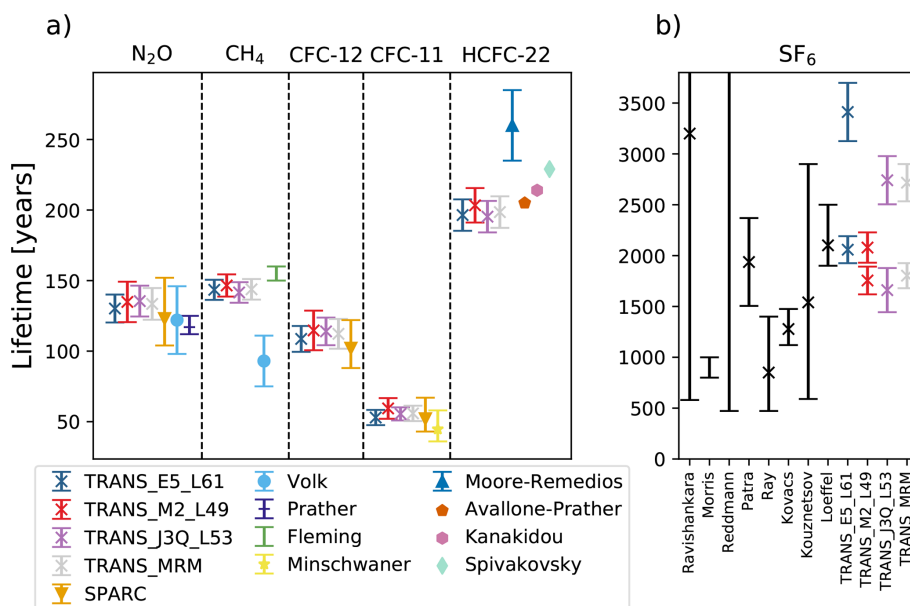
Figure 9. Lifetime of atmospheric trace gases averaged over 2002–2012. The SF$_6$ lifetimes from the literature are shown as error bars without marker point if only a range was given, or as an error bar with a marker at the most likely lifetime value, or as a single point if only one value was given. The lifetimes for CH$_4$ and HCFC-22 are integrated only over stratospheric levels (see methods).

viation over 10 years. Given the large differences in seasonal variability for SF$_6$ lifetime between the three reanalyses (see Fig. 10) the results have been split up into the averages of the maxima (equinoxes) and minima (solstices) of the time series. The BASCOE averages show good agreement with the result from the transient reference simulation (REF) and the simulation nudged to ERA-Interim in Loeffel et al. (2022), using the global chemistry climate model EMAC. This is especially true for the simulation driven by JRA-3Q. The lifetime from the simulation driven by MERRA2 is similar to the lifetime from the time slice simulation (TS2000) in Loeffel et al. (2022), which uses fixed climate conditions from the year 2000. The lifetime derived from the ERA5-driven simulation is closer to their CSS simulation, which uses the same climate conditions as the transient reference simulation, but sets the concentrations of the SF$_6$ reactant species to 1950 levels. Due to the considerable tropospheric growth rates of SF$_6$ of around 5 % yr^{-1}, the instantaneous lifetime of this species is expected to be significantly larger than the steady-state lifetime. We compute a correction for the instantaneous lifetime of SF$_6$, using the formula by Minschwaner et al. (2013) mentioned above, assuming an age of air of 8 years in the region of maximum loss. This gives an estimate for the steady-state lifetime that is 20 %–30 % shorter than the instantaneous lifetime. Additionally, a one day simulation was done to assess the sensitivity to the volume mixing ratios of SF$_6$ on the lifetime. Given that BASCOE slightly underestimates the SF$_6$ concentrations (see Figs. 5 and 6), we increased the initial conditions of SF$_6$ by 10 % and ran the model for one day to analyse the impact of the volume mixing ratios. We found

that the instantaneous lifetime of one snapshot of the model decreased by about 30 years. Similarly, if the volume mixing ratios were decreased by 10 %, the lifetime increased by about 40 years. This difference is small compared to the total lifetime, on the order of 1 %, which indicates that the chemistry of SF$_6$ is more or less linear, i.e., not highly coupled with other gases. This implies that the lifetime computation is relatively independent of potential errors in the volume mixing ratios.

For N$_2$O, CH$_4$, CFC-11, CFC-12 and HCFC-22, the lifetimes derived from the three different simulations are closely aligned (see Fig. 9a), indicating that there is little sensitivity to meteorology for these species, possibly due to good agreement between the reanalyses at altitudes where the species are destroyed. However, TRANS_E5_L61 consistently produces a slightly lower lifetime than TRANS_M2_L49, TRANS_J3Q_L53 being often in between. For SF$_6$ there are relatively large differences between the three values. This could be explained by the lack of stratospheric and mesospheric observations to constrain the reanalyses in the region where SF$_6$ chemistry is important, as well as the differences in the sponge layers between the three reanalyses. Also, contrary to the 5 other species, SF$_6$ lifetime from TRANS_E5_L61 is significantly longer than the lifetime from TRANS_J3Q_L53 and TRANS_M2_L49. We hypothesize that SF$_6$ spends less time in the mesosphere due to the faster circulation with ERA5 and is therefore able to return to the stratosphere via recirculation, resulting in higher volume mixing ratios in the stratosphere and thus a longer lifetime.

Table 4. Average instantaneous lifetime (years) of six long-lived trace gases from the different BASCOE simulations for the period 2002–2012 and their 1σ standard deviation. For CH_4 and HCFC-22, stratospheric lifetime is shown, while global atmospheric lifetime is shown for the other species.

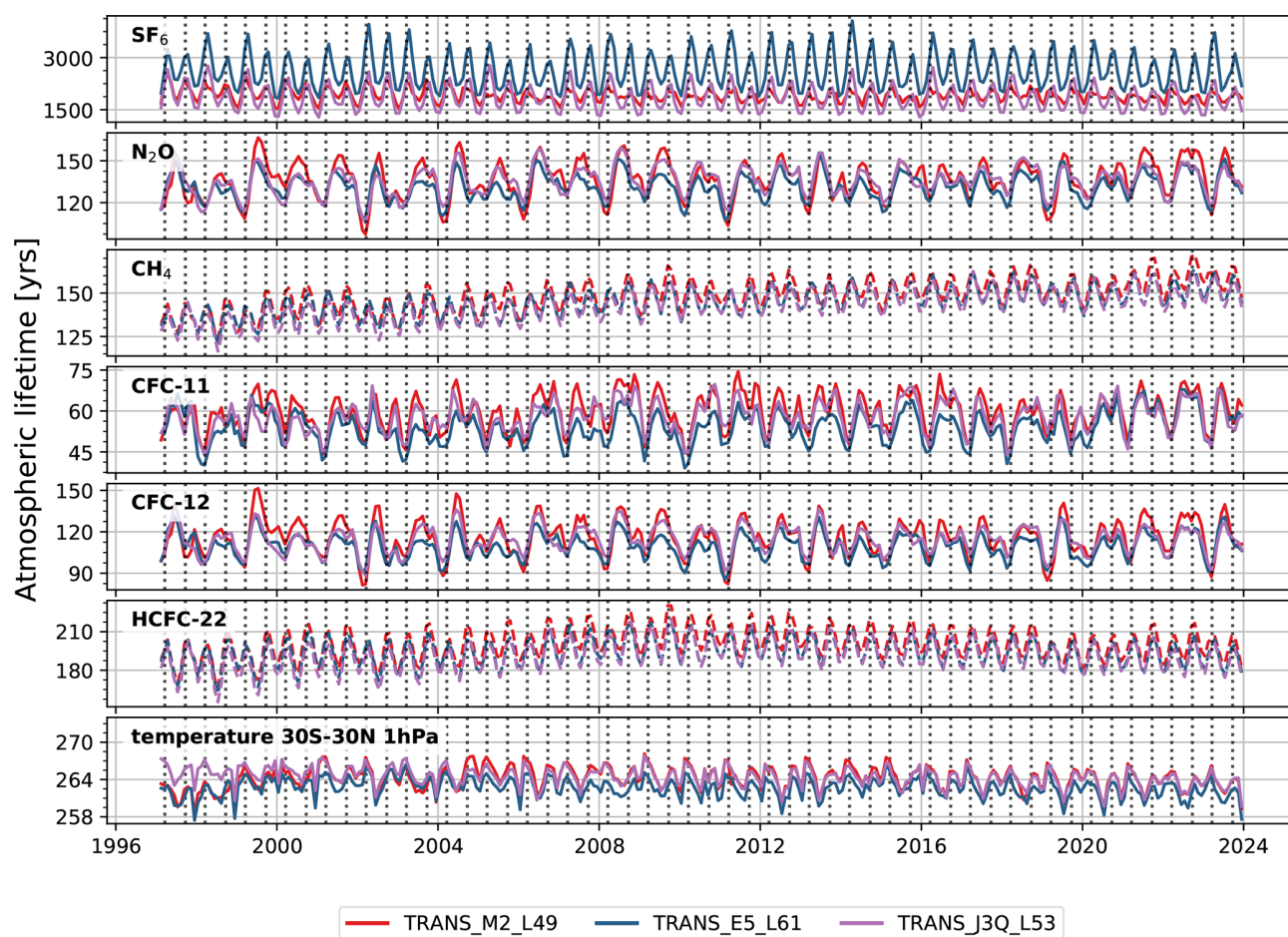| Experiment	N_2O	CH_4	CFC-11	CFC-12	HCFC-22	SF_6	SF_6 max	SF_6 min
TRANS_E5_L61	130 ± 10	144 ± 7	52 ± 5	108 ± 9	198 ± 11	2646 ± 532	3412 ± 286	2058 ± 133
TRANS_M2_L49	135 ± 14	147 ± 8	59 ± 7	115 ± 14	204 ± 12	1909 ± 182	2079 ± 149	1755 ± 136
TRANS_J3Q_L53	135 ± 11	142 ± 7	56 ± 5	114 ± 10	195 ± 11	2147 ± 459	2741 ± 237	1660 ± 217
TRANS_MRM	133 ± 11	144 ± 7	56 ± 5	112 ± 11	199 ± 11	2235 ± 372	2717 ± 183	1802 ± 123

Figure 10. Global atmospheric lifetime (solid lines) or stratospheric lifetime (dashed lines) of different species computed from BASCOE simulation driven by ERA5 (blue lines), MERRA2 (red lines) and JRA-3Q (purple lines).

The time series of the lifetime of all six species and the tropical temperature at 1 hPa are shown in Fig. 10. There is an increasing trend in the lifetime of CH_4, consistent with predictions from Li et al. (2022), but not for the other species, while Prather et al. (2023) found a decreasing trend of N_2O lifetimes. There is no clear trend in the SF_6 lifetime despite the strong growth of SF_6, in contrast to the increasing trends in the reference simulation and the projected simulation from Loeffel et al. (2022). Instead, the lifetimes are steady over the entire simulation range, similar to the time-slice simulation

in Loeffel et al. (2022), which was used to compute a steady-state lifetime. In the time series, a semi-annual oscillation (SAO, Reed, 1965) is observed. The SAO is more apparent and more regular for CH_4 and HCFC-22 than for CFC-11, CFC-12 and N_2O. SAO's in the winds and temperature have been previously observed near the stratopause around 1 hPa and near the mesopause at around 0.01 hPa (Shangguan and Wang, 2023). The SAO in the stratosphere is thought to be driven by Kelvin waves, caused by convection in the tropics, and linked to the passage of the Sun across the equa-

tor that happens twice per year and the absorption of solar UV by ozone in the stratosphere. The origin of the mesospheric SAO is not well understood, but it is considered that the mesospheric SAO is driven by selective transmission of inertia-gravity waves and there appears to be a lag between the stratospheric and the mesospheric SAO (Richter and Garcia, 2006). The temperature is plotted in the tropics at 1 hPa, the region where the SAO is the strongest (Shangguan and Wang, 2023). While similar patterns are observed between the temperature at 1 hPa in the tropics and the time series of the lifetime, the link between both quantities is not clear. For SF$_6$, the amplitude of the seasonal variation of the lifetime is larger for TRANS_E5_L61 than for the two other simulations. This could be related to the stronger seasonal cycle in the total tropical upwelling of ERA5 with respect to MERRA2 (SPARC, 2022, Chap. 5). For SF$_6$ the maxima in the lifetime happen in spring and autumn, around the equinoxes, while the minima are in summer and winter around the solstices. For N$_2$O the occurrence of peaks and valleys is reversed, with the maxima around the solstices and the minima around the equinoxes. CH$_4$ and HCFC-22 are similar to SF$_6$, while CFC-11 and CFC-12 are more similar to N$_2$O.

6   Conclusions

The chemistry of SF$_6$ has been implemented in the Belgian Assimilation System for Chemical ObsErvations (BASCOE). Three model simulations have been carried out, driven by three recent meteorological reanalyses (ERA5, MERRA2 and JRA-3Q) that include the mesosphere where SF$_6$ is destroyed via auto-attachment with electrons. These simulations show a relatively good agreement with MIPAS and ACE-FTS satellite observations in the middle and low stratosphere with differences generally within $\pm 10\,\%$ for SF$_6$ volume mixing ratios and mostly within the estimated instrumental differences for all six species below 10 hPa. For SF$_6$, the simulation driven by MERRA2 has a slightly smaller differences with respect to MIPAS than those driven by ERA5 and JRA-3Q. The instantaneous global atmospheric lifetime of SF$_6$ was computed and compared with published results to further assess the impact of the choice of meteorology in the mesosphere where satellite observations provide little information. The lifetime was also computed for the other long-lived species. The computed lifetime of SF$_6$ – 2646 ± 532 (1σ) years (ERA5), 1909 ± 182 (1σ) years (MERRA2) and 2147 ± 459 (1σ) years (JRA-3Q) – is consistent with recent results by Loeffel et al. (2022), but demonstrates the sensitivity of SF$_6$-derived transport diagnostics to the underlying meteorological data. For the other trace gases, the lifetimes from the three simulations are in good agreement between themselves and with published results, which confirms the validity of our lifetime calculation. A semi-annual oscillation is observed in the time evolution of the lifetimes

of all six species, which exhibits similar patterns as tropical stratospheric temperature variations. A follow-up study is necessary to further investigate the differences in stratospheric transport among the three reanalyses in order to explain the differences in seasonal variation observed in the lifetime. With this model update, BASCOE is ready to perform further transport studies based on SF$_6$ diagnostics.

Appendix A: Computation of the reduced grids

This appendix describes the procedure to construct a vertical grid with reduced resolution for the reanalyses. The reanalyses used in this work are defined on a hybrid sigma-pressure grid. The pressure at level interface $p_{\mathrm{mid}}(i)$ is defined by the model level parameters $A_p(i)$ and $B_p(i)$ as follows:

$$p_{\mathrm{mid}}(i) = A_p(i) + B_p(i) \cdot p_{\mathrm{surf}} \qquad (A1)$$

with p_{surf} being the surface pressure and $i = 1, \mathrm{nlev}$ is the level index and nlev is the number of model levels. The reduced grids are obtained as follows, see also the illustration in Fig. A1:

- Step 1: For several altitudes between 5 and 90 km, values of the desired vertical resolution dz were provided, hereby aiming to stay close to the native resolution in the upper levels and reducing the resolution in the troposphere.

- Step 2: These proposed altitude-resolution points were then fitted with a polynomial.

- Step 3: Starting from the surface, the vertical resolution at the lowest level is calculated using this polynomial, and this defines the altitude of the lowest level. Then level $i + 1$ was calculated by incrementing level i with the vertical interval dz from the polynomial at level i, ensuring that the top levels correspond to the top levels of the reanalysis.

- Step 4: Then the native A_p and B_p are interpolated to the new vertical grid using a log-pressure approximation for the altitude. From the new A_p and B_p coefficients, the sigma-pressure levels were computed.
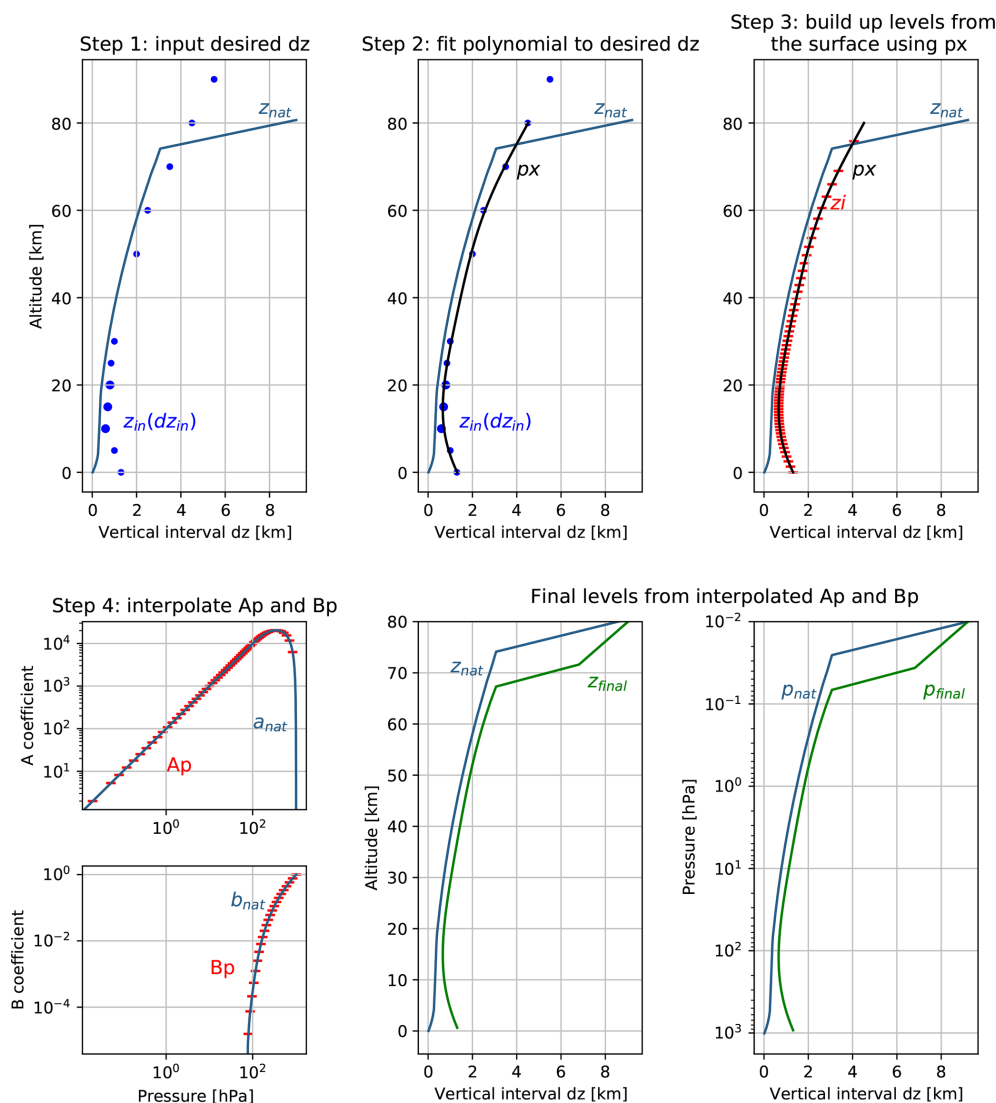
Figure A1. Workflow to construct a new grid for the reanalyses with desired vertical resolution (see text for details).

Author contributions. SV executed the implementation of the chemistry, carried out the simulations and visualized and interpreted the results. QE and EM provided the idea for the study, supervised the work and contributed to the interpretation of the results and revising of the manuscript. EM is senior research associate with F.R.S.-FNRS. SC and MOdb helped with the interpretation of the results and provided feedback on the manuscript. TR provided support in the implementation of SF$_6$ chemistry in BASCOE and provided feedback on preliminary results. GS provided support in the use of MIPAS data sets. RE provided the EMAC data set and provided feedback on preliminary results.

The peer-review process was guided by an independent editor, and the authors also have no other competing interests to declare.

Disclaimer. Publisher's note: Copernicus Publications remains neutral with regard to jurisdictional claims made in the text, published maps, institutional affiliations, or any other geographical representation in this paper. The authors bear the ultimate responsibility for providing appropriate place names. Views expressed in the text are those of the authors and do not necessarily reflect the views of the publisher.

Special issue statement. This article is part of the special issue "The SPARC Reanalysis Intercomparison Project (S-RIP) Phase 2 (ACP/WCD inter-journal SI)". It is not associated with a conference.

Review statement. This paper was edited by Jens-Uwe Grooß and reviewed by two anonymous referees.

References

Abalos, M., Calvo, N., Benito-Barca, S., Garny, H., Hardiman, S. C., Lin, P., Andrews, M. B., Butchart, N., Garcia, R., Orbe, C., Saint-Martin, D., Watanabe, S., and Yoshida, K.: The Brewer–Dobson circulation in CMIP6, Atmos. Chem. Phys., 21, 13571–13591, https://doi.org/10.5194/acp-21-13571-2021, 2021.

ACE-FTS: Level-2 Data, Version 5.3, https://uwaterloo.ca/atmospheric-chemistry-experiment/ (last access: 5 January 2026), 2025.

Austin, J. and Li, F.: On the relationship between the strength of the Brewer–Dobson circulation and the age of stratospheric air, Geophys. Res. Lett., 33, https://doi.org/10.1029/2006GL026867, 2006.

Avallone, L. M. and Prather, M. J.: Tracer-tracer correlations: Three-dimensional model simulations and comparisons to observations, J. Geophys. Res.-Atmos., 102, 19233–19246, https://doi.org/10.1029/97JD01123, 1997.

Bernath, P. F., McElroy, C. T., Abrams, M. C., Boone, C. D., Butler, M., Camy-Peyret, C., Carleer, M., Clerbaux, C., Coheur, P.-F., Colin, R., De Cola, P., De Mazière, M., Drummond, J. R., Dufour, D., Evans, W. F. J., Fast, H., Fussen, D., Gilbert, K., Jennings, D. E., Llewellyn, E. J., Lowe, R. P., Mahieu, E., McConnell, J. C., McHugh, M., McLeod, S. D., Michaud, R., Midwinter, C., Nassar, R., Nichitiu, F., Nowlan, C., Rinsland, C. P., Rochon, Y. J., Rowlands, N., Semeniuk, K., Simon, P., Skelton, R., Sloan, J. J., Soucy, M.-A., Strong, K., Tremblay, P., Turnbull, D., Walker, K. A., Walkty, I., Wardle, D. A., Wehrle, V., Zander, R., and Zou, J.: Atmospheric chemistry experiment (ACE): mission overview, Geophys. Res. Lett., 32, https://doi.org/10.1029/2005GL022386, 2005.

Brasseur, G. P. and Solomon, S.: Aeronomy of the Middle Atmosphere, https://doi.org/10.1007/1-4020-3824-0_2, 2005.

Brewer, A.: Evidence for a world circulation provided by the measurements of helium and water vapour distribution in the stratosphere, Q. J. Roy. Meteor. Soc., 75, 351–363, https://doi.org/10.1002/qj.49707532603, 1949.

Burkholder, J., Sander, S., Abbatt, J., Barker, J., Huie, R., Kolb, C., Kurylo, M., Orkin, V., Wilmouth, D., and Wine, P.: Chemical kinetics and photochemical data for use in atmospheric studies: evaluation number 18, Tech. rep., Jet Propulsion Laboratory, National Aeronautics and Space, Pasadena, CA, https://jpldataeval.jpl.nasa.gov/ (last access: 5 January 2026), 2015.

Butchart, N.: The Brewer–Dobson circulation, Rev. Geophys., 52, 157–184, https://doi.org/10.1002/2013RG000448, 2014.

Butchart, N., Scaife, A. A., Bourqui, M., Grandpré, J., Hare, S. H., Kettleborough, J., Langematz, U., Manzini, E., Sassi, F., Shibata, K., Shindell, D., and Sigmond, M.: Simulations of anthropogenic change in the strength of the Brewer–Dobson circulation, Clim. Dynam., 27, 727–741, https://doi.org/10.1007/s00382-006-0162-4, 2006.

Chabrillat, S., Vigouroux, C., Christophe, Y., Engel, A., Errera, Q., Minganti, D., Monge-Sanz, B. M., Segers, A., and Mahieu, E.: Comparison of mean age of air in five reanalyses using the BASCOE transport model, Atmos. Chem. Phys., 18, 14715–14735, https://doi.org/10.5194/acp-18-14715-2018, 2018.

Damian, V., Sandu, A., Damian, M., Potra, F., and Carmichael, G. R.: The kinetic preprocessor KPP-a software environment for solving chemical kinetics, Comput. Chem. Eng., 26, 1567–1579, https://doi.org/10.1016/S0098-1354(02)00128-X, 2002.

Datskos, P. G., Carter, J. G., and Christophorou, L. G.: Photodetachment of SF$_6$, Chem. Phys. Lett., 239, 38–43, https://doi.org/10.1016/0009-2614(95)00417-3, 1995.

de la Paz, M., Velo, A., Steinfeldt, R., and Pérez, F. F.: The Unaccounted Oceanic Sink of Anthropogenic Nitrous Oxide and Its Relationship With Anthropogenic Carbon Dioxide, 39, https://doi.org/10.1029/2024gb008417, 2025.

Dietmüller, S., Eichinger, R., Garny, H., Birner, T., Boenisch, H., Pitari, G., Mancini, E., Visioni, D., Stenke, A., Revell, L., Rozanov, E., Plummer, D. A., Scinocca, J., Jöckel, P., Oman, L., Deushi, M., Kiyotaka, S., Kinnison, D. E., Garcia, R., Morgenstern, O., Zeng, G., Stone, K. A., and Schofield, R.: Quantifying the effect of mixing on the mean age of air in CCMVal-2 and CCMI-1 models, Atmos. Chem. Phys., 18, 6699–6720, https://doi.org/10.5194/acp-18-6699-2018, 2018.

Dobson, G. M. B.: Origin and distribution of the polyatomic molecules in the atmosphere, Proceedings of the Royal Society of London. Series A. Mathematical and Physical Sciences, 236, 187–193, https://doi.org/10.1098/rspa.1956.0127, 1956.

Dobson, G. M. B., Kimball, H., and Kidson, E.: Observations of the amount of ozone in the earth's atmosphere, and its relation to other geophysical conditions – Part IV, Proc. R. Soc. London A, 129, 411–433, https://doi.org/10.1098/rspa.1930.0165, 1930.

Eichinger, R., Dietmüller, S., Garny, H., Šácha, P., Birner, T., Bönisch, H., Pitari, G., Visioni, D., Stenke, A., Rozanov, E., Revell, L., Plummer, D. A., Jöckel, P., Oman, L., Deushi, M., Kinnison, D. E., Garcia, R., Morgenstern, O., Zeng, G., Stone, K. A., and Schofield, R.: The influence of mixing on the stratospheric age of air changes in the 21st century, Atmos. Chem. Phys., 19, 921–940, https://doi.org/10.5194/acp-19-921-2019, 2019.

Errera, Q., Daerden, F., Chabrillat, S., Lambert, J. C., Lahoz, W. A., Viscardy, S., Bonjean, S., and Fonteyn, D.: 4D-Var assimilation of MIPAS chemical observations: ozone and ni-

trogen dioxide analyses, Atmos. Chem. Phys., 8, 6169–6187, https://doi.org/10.5194/acp-8-6169-2008, 2008.

Errera, Q., Chabrillat, S., Christophe, Y., Debosscher, J., Hubert, D., Lahoz, W., Santee, M. L., Shiotani, M., Skachko, S., von Clarmann, T., and Walker, K.: Technical note: Reanalysis of Aura MLS chemical observations, Atmos. Chem. Phys., 19, 13647–13679, https://doi.org/10.5194/acp-19-13647-2019, 2019.

Fischer, H., Birk, M., Blom, C., Carli, B., Carlotti, M., von Clarmann, T., Delbouille, L., Dudhia, A., Ehhalt, D., Endemann, M., Flaud, J. M., Gessner, R., Kleinert, A., Koopman, R., Langen, J., López-Puertas, M., Mosner, P., Nett, H., Oelhaf, H., Perron, G., Remedios, J., Ridolfi, M., Stiller, G., and Zander, R.: MIPAS: an instrument for atmospheric and climate research, Atmos. Chem. Phys., 8, 2151–2188, https://doi.org/10.5194/acp-8-2151-2008, 2008.

Fleming, E. L., George, C., Heard, D. E., Jackman, C. H., Kurylo, M. J., Mellouki, W., Orkin, V. L., Swartz, W. H., Wallington, T. J., Wine, P. H., and Burkholder, J. B.: The impact of current CH$_4$ and N$_2$O atmospheric loss process uncertainties on calculated ozone abundances and trends, J. Geophys. Res., 120, 5267–5293, https://doi.org/10.1002/2014JD022067, 2015.

Garny, H., Birner, T., Bönisch, H., and Bunzel, F.: The effects of mixing on age of air, 119, 7015–7034, https://doi.org/10.1002/2013jd021417, 2014.

Garny, H., Eichinger, R., Laube, J. C., Ray, E. A., Stiller, G. P., Bönisch, H., Saunders, L., and Linz, M.: Correction of stratospheric age of air (AoA) derived from sulfur hexafluoride (SF$_6$) for the effect of chemical sinks, Atmos. Chem. Phys., 24, 4193–4215, https://doi.org/10.5194/acp-24-4193-2024, 2024a.

Garny, H., Ploeger, F., Abalos, M., Bönisch, H., Castillo, A. E., von Clarmann, T., Diallo, M., Engel, A., Laube, J. C., Linz, M., Neu, J. L., Podglajen, A., Ray, E., Rivoire, L., Saunders, L. N., Stiller, G., Voet, F., Wagenhäuser, T., and Walker, K. A.: Age of stratospheric air: Progress on processes, observations, and long-term trends, Rev. Geophys., 62, e2023RG000832, https://doi.org/10.1029/2023RG000832, 2024b.

Gelaro, R., McCarty, W., Suárez, M. J., Todling, R., Molod, A., Takacs, L., Randles, C. A., Darmenov, A. and Bosilovich, M. G. and Reichle, R. and Wargan, K., Coy, L., Cullather, R., Draper, C., Akella, S., Buchard, V., Conaty, A., da Silva, A. M., Gu, W., Kim, G.-K., Koster, R., Lucchesi, R., Merkova, D., Nielsen, J. E. and Partyka, G. and Pawson, S. and Putman, W., Rienecker, M., Schubert, S. D., Sienkiewicz, M., and Zhao, B.: The modern-era retrospective analysis for research and applications, version 2 (MERRA-2), Journal of Climate, 30, 5419–5454, https://doi.org/10.1175/JCLI-D-16-0758.1, 2017.

Gidden, M. J., Riahi, K., Smith, S. J., Fujimori, S., Luderer, G., Kriegler, E., van Vuuren, D. P., van den Berg, M., Feng, L., Klein, D., Calvin, K., Doelman, J. C., Frank, S., Fricko, O., Harmsen, M., Hasegawa, T., Havlik, P., Hilaire, J., Hoesly, R., Horing, J., Popp, A., Stehfest, E., and Takahashi, K.: Global emissions pathways under different socioeconomic scenarios for use in CMIP6: a dataset of harmonized emissions trajectories through the end of the century, Geosci. Model Dev., 12, 1443–1475, https://doi.org/10.5194/gmd-12-1443-2019, 2019.

Hall, T. M. and Plumb, R. A.: Age as a diagnostic of stratospheric transport, J. Geophys. Res., 99, 1059–1070, https://doi.org/10.1029/93JD03192, 1994.

Hardiman, S. C., Butchart, N., and Calvo, N.: The morphology of the Brewer–Dobson circulation and its response to climate change in CMIP5 simulations: Morphology of the Brewer–Dobson Circulation, 140, 1958–1965, https://doi.org/10.1002/qj.2258, 2013.

Harnisch, J., Borchers, R., Fabian, P., and Maiss, M.: Cf4 and the age of mesospheric and polar vortex air, Geophys. Res. Lett., 26, 295–298, https://doi.org/10.1029/1998GL900307, 1999.

Hersbach, H., Bell, D., Berrisford, P., Hirahara, S., Horányi, A., Muñoz-Sabater, J., Nicolas, J., Peubey, C., Radu, R., Schepers, D., Simmons, A., Soci, C., Abdalla, S., Abellan, X., Balsamo, G., Bechtold, P., Biavati, G., Bidlot, J., Bonavita, M., De Chiara, G., Dahlgren, P., Dee, D., Diamantakis, M., Dragani, R., Flemming, J., Forbes, R., Fuentes, M., Geer, A., Haimberger, L., Healy, S., Hogan, R. J., Hólm, E., Janisková, M., Keeley, S., Laloyaux, P., Lopez, P., Lupu, C., Radnoti, G., de Rosnay, P., Rozum, I., Vamborg, F., Villaume, S., and Thépaut, J.-N.: The ERA5 global reanalysis, Q. J. Roy. Meteor. Soc., 146, 1999–2049, https://doi.org/10.1002/qj.3803, 2020.

Ingólfsson, O., Illenberger, E., and Schmidt, W.-F.: Photodetachment from anions in a drift at 337 nm cell. Application to SF, Int. J. Mass Spectrom., 139, 103–110, https://doi.org/10.1016/0168-1176(94)90020-5, 1994.

Kanakidou, M., Dentener, F. J., and Crutzen, P. J.: A global three-dimensional study of the fate of HCFCs and HFC-134a in the troposphere, J. Geophys. Res.-Atmos., 100, 18781–18801, https://doi.org/10.1029/95JD01919, 1995.

Ko, M. K., Sze, N. D., Wang, W.-C., Shia, G., Goldman, A., Murcray, F. J., Murcray, D. G., and Rinsland, C. P.: Atmospheric sulfur hexafluoride: Sources, sinks and greenhouse warming, J. Geophys. Res.-Atmos., 98, 10499–10507, https://doi.org/10.1029/93JD00228, 1993.

Kolonjari, F., Sheese, P. E., Walker, K. A., Boone, C. D., Plummer, D. A., Engel, A., Montzka, S. A., Oram, D. E., Schuck, T., Stiller, G. P., and Toon, G. C.: Validation of Atmospheric Chemistry Experiment Fourier Transform Spectrometer (ACE-FTS) chlorodifluoromethane (HCFC-22) in the upper troposphere and lower stratosphere, Atmos. Meas. Tech., 17, 2429–2449, https://doi.org/10.5194/amt-17-2429-2024, 2024.

Kosaka, Y., Kobayashi, S., Harada, Y., Kobayashi, C., Naoe, H., Yoshimoto, K., Harada, M., Goto, N., Chiba, J., Miyaoka, K., Sekiguchi, R., Deushi, M., Kamahori, H., Nakaegawa, T., Tanaka, T. Y., Tokuhiro, T., Sato, Y., Matsushita, Y., and Onogi, K.: The JRA-3Q reanalysis, Journal of the Meteorological Society of Japan. Ser. II, 102, 49–109, https://doi.org/10.2151/jmsj.2024-004, 2024.

Kouznetsov, R., Sofiev, M., Vira, J., and Stiller, G.: Simulating age of air and the distribution of SF$_6$ in the stratosphere with the SILAM model, Atmos. Chem. Phys., 20, 5837–5859, https://doi.org/10.5194/acp-20-5837-2020, 2020.

Kovács, T., Feng, W., Totterdill, A., Plane, J. M. C., Dhomse, S., Gómez-Martín, J. C., Stiller, G. P., Haenel, F. J., Smith, C., Forster, P. M., García, R. R., Marsh, D. R., and Chipperfield, M. P.: Determination of the atmospheric lifetime and global warming potential of sulfur hexafluoride using a three-dimensional model, Atmos. Chem. Phys., 17, 883–898, https://doi.org/10.5194/acp-17-883-2017, 2017.

Krey, P., Lagomarsino, R., and Toonkel, L.: Gaseous halogens in the atmosphere in 1975, J. Geophys. Res., 82, 1753–1766, https://doi.org/10.1029/JC082i012p01753, 1977.

Laeng, A., Plieninger, J., von Clarmann, T., Grabowski, U., Stiller, G., Eckert, E., Glatthor, N., Haenel, F., Kellmann, S., Kiefer, M., Linden, A., Lossow, S., Deaver, L., Engel, A., Hervig, M., Levin, I., McHugh, M., Noël, S., Toon, G., and Walker, K.: Validation of MIPAS IMK/IAA methane profiles, Atmos. Meas. Tech., 8, 5251–5261, https://doi.org/10.5194/amt-8-5251-2015, 2015.

Li, Q., Fernandez, R. P., Hossaini, R., Iglesias-Suarez, F., Cuevas, C. A., Apel, E. C., Kinnison, D. E., Lamarque, J.-F., and Saiz-Lopez, A.: Reactive halogens increase the global methane lifetime and radiative forcing in the 21st century, Nat. Commun., 13, 2768, https://doi.org/10.1038/s41467-022-30456-8, 2022.

Lin, S.-J. and Rood, R. B.: Multidimensional flux-form semi-Lagrangian transport schemes, Monthly Weather Review, 124, 2046–2070, https://doi.org/10.1175/1520-0493(1996)124<2046:MFFSLT>2.0.CO;2, 1996.

Loeffel, S., Eichinger, R., Garny, H., Reddmann, T., Fritsch, F., Versick, S., Stiller, G., and Haenel, F.: The impact of sulfur hexafluoride (SF$_6$) sinks on age of air climatologies and trends, Atmos. Chem. Phys., 22, 1175–1193, https://doi.org/10.5194/acp-22-1175-2022, 2022.

Meinshausen, M., Vogel, E., Nauels, A., Lorbacher, K., Meinshausen, N., Etheridge, D. M., Fraser, P. J., Montzka, S. A., Rayner, P. J., Trudinger, C. M., Krummel, P. B., Beyerle, U., Canadell, J. G., Daniel, J. S., Enting, I. G., Law, R. M., Lunder, C. R., O'Doherty, S., Prinn, R. G., Reimann, S., Rubino, M., Velders, G. J. M., Vollmer, M. K., Wang, R. H. J., and Weiss, R.: Historical greenhouse gas concentrations for climate modelling (CMIP6), Geosci. Model Dev., 10, 2057–2116, https://doi.org/10.5194/gmd-10-2057-2017, 2017.

Miller, T. M., Miller, A. E. S., Paulson, J. F., and Liu, X.: Thermal electron attachment to SF$_4$ and SF$_6$, 100, 8841–8848, https://doi.org/10.1063/1.466738, 1994.

Minschwaner, K., Hoffmann, L., Brown, A., Riese, M., Müller, R., and Bernath, P. F.: Stratospheric loss and atmospheric lifetimes of CFC-11 and CFC-12 derived from satellite observations, Atmos. Chem. Phys., 13, 4253–4263, https://doi.org/10.5194/acp-13-4253-2013, 2013.

MIPAS: Level-2 Data, Version 8, https://www.imk-asf.kit.edu/english/308.php (last access: 5 January 2026), 2019.

Moore, D. P. and Remedios, J. J.: Growth rates of stratospheric HCFC-22, Atmos. Chem. Phys., 8, 73–82, https://doi.org/10.5194/acp-8-73-2008, 2008.

Morris, R. A., Miller, T. M., Viggiano, A. A., Paulson, J. F., Solomon, S., and Reid, G.: Effects of electron and ion reactions on atmospheric lifetimes of fully fluorinated compounds, https://doi.org/10.1029/94JD02399, 1995.

Patra, P. K., Lal, S., Subbaraya, B. H., Jackman, C. H., and Rajaratnam, P.: Observed vertical profile of sulphur hexafluoride (SF$_6$) and its atmospheric applications, Journal of Geophysical Research Atmospheres, 102, 8855–8859, 1997.

Ploeger, F., Diallo, M., Charlesworth, E., Konopka, P., Legras, B., Laube, J. C., Grooß, J.-U., Günther, G., Engel, A., and Riese, M.: The stratospheric Brewer–Dobson circulation inferred from age of air in the ERA5 reanalysis, Atmos. Chem. Phys., 21, 8393–8412, https://doi.org/10.5194/acp-21-8393-2021, 2021.

Plumb, R. A. and Ko, M. K. W.: Interrelationships between mixing ratios of long-lived stratospheric constituents, 97, 10145–10156, https://doi.org/10.1029/92jd00450, 1992.

Prather, M. J., Froidevaux, L., and Livesey, N. J.: Observed changes in stratospheric circulation: decreasing lifetime of N$_2$O, 2005–2021, Atmos. Chem. Phys., 23, 843–849, https://doi.org/10.5194/acp-23-843-2023, 2023.

Prignon, M.: Stratospheric circulation changes: investigations using multidecadal observations and simulations of inorganic fluorine, Ph. D. thesis, ULiège – Université de Liège, Eprint: https://orbi.uliege.be/2268/260555, 2021.

Prignon, M., Chabrillat, S., Friedrich, M., Smale, D., Strahan, S. E., Bernath, P. F., Chipperfield, M. P., Dhomse, S. S., Feng, W., Minganti, D., Servais, C., and Mahieu, E.: Stratospheric fluorine as a tracer of circulation changes: Comparison between infrared remote-sensing observations and simulations with five modern reanalyses, J. Geophys. Res.-Atmos., 126, e2021JD034995, https://doi.org/10.1029/2021jd034995, 2021.

Ravishankara, A. R., Solomon, S., Turnipseed, A. A., and Warren, R. F.: Atmospheric Lifetimes of Long-Lived Halogenated Species, 194–199, https://doi.org/10.1126/science.259.5092.194, 1993.

Ray, E. A., Moore, F. L., Elkins, J. W., Rosenlof, K. H., Laube, J. C., Röckmann, T., Marsh, D. R., and Andrews, A. E.: Quantification of the SF$_6$ lifetime based on mesospheric loss measured in the stratospheric polar vortex, J. Geophys. Res., 122, 4626–4638, https://doi.org/10.1002/2016JD026198, 2017.

Reddmann, T., Ruhnke, R., and Kouker, W.: Three-dimensional model simulations of SF$_6$ with mesospheric chemistry, Journal of Geophysical Research Atmospheres, 106, 14525–14537, https://doi.org/10.1029/2000JD900700, 2001.

Reed, R. J.: The present status of the 26 month oscillation, B. Am. Meteorol. Soc., 46, 374–387, 1965.

Richter, J. H. and Garcia, R. R.: On the forcing of the Mesospheric Semi-Annual Oscillation in the Whole Atmosphere Community Climate Model, 33, https://doi.org/10.1029/2005gl024378, 2006.

Shangguan, M. and Wang, W.: Analysis of temperature Semi-Annual Oscillations (SAO) in the middle atmosphere, Remote Sensing, 15, 857, https://doi.org/10.3390/rs15030857, 2023.

Sheese, P. E., Walker, K. A., Boone, C. D., Bernath, P. F., Froidevaux, L., Funke, B., Raspollini, P., and von Clarmann, T.: ACE-FTS ozone, water vapour, nitrous oxide, nitric acid, and carbon monoxide profile comparisons with MIPAS and MLS, J. Quant. Spectrosc. Radiat. Transfer, 186, 63–80, https://doi.org/10.1016/j.jqsrt.2016.06.026, 2017.

SPARC: SPARC Report on the Lifetimes of Stratospheric Ozone-Depleting Substances, Their Replacements, and Related Species. edited by: Ko, M. K. W., Newman, P. A., Reimann, S., and Strahan, S. E., SPARC Report No. 6, WCRP-15/2013, https://www.sparc-climate.org/publications/sparc-reports/ (last access: 5 January 2026), 2013.

SPARC: The SPARC Data Initiative: Assessment of stratospheric trace gas and aerosol climatologies from satellite limb sounders, Tech. Rep. 8, SPARC, wCRP-5/2017, https://www.sparc-climate.org/publications/sparc-reports/ (last access: 5 January 2026), https://doi.org/10.3929/ethz-a-010863911, 2017.

SPARC: SPARC Reanalysis Intercomparison Project (S-RIP) Final Report, Tech. Rep. 10, SPARC, https://doi.org/10.17874/800dee57d13, 2022.

Spivakovsky, C. M., Logan, J. A., Montzka, S. A., Balkanski, Y. J., Foreman-Fowler, M., Jones, D. B. A., Horowitz, L. W., Fusco, A. C., Brenninkmeijer, C. A. M., Prather, M. J., Wofsy, S. C., and McElroy, M. B.: Three-dimensional climatological distribution of tropospheric OH: Update and evaluation, J. Geophys. Res.-Atmos., 105, 8931–8980, https://doi.org/10.1029/1999JD901006, 2000.

Strahan, S. E. and Polansky, B. C.: Meteorological implementation issues in chemistry and transport models, Atmos. Chem. Phys., 6, 2895–2910, https://doi.org/10.5194/acp-6-2895-2006, 2006.

Totterdill, A., Kovács, T., Martín, J. C. G., Feng, W., and Plane, J. M.: Mesospheric Removal of Very Long-Lived Greenhouse Gases SF$_6$ and CFC-115 by Metal Reactions, Lyman-α Photolysis, and Electron Attachment, J. Phys. Chem. A, 119, 2016–2025, https://doi.org/10.1021/jp5123344, 2015.

Vervalcke, S.: BASCOE CTM simulations driven by ERA5, MERRA2 and JRA-3Q monthly zonal means, Zenodo [data set], https://doi.org/10.5281/zenodo.17751040, 2025.

Voet, F., Ploeger, F., Laube, J., Preusse, P., Konopka, P., Grooß, J.-U., Ungermann, J., Sinnhuber, B.-M., Höpfner, M., Funke, B., Wetzel, G., Johansson, S., Stiller, G., Ray, E., and Hegglin, M. I.: On the estimation of stratospheric age of air from correlations of multiple trace gases, Atmos. Chem. Phys., 25, 3541–3565, https://doi.org/10.5194/acp-25-3541-2025, 2025.

Volk, C. M., Elkins, J. W., Fahey, D. W., Dutton, G. S., Gilligan, J. M., Loewenstein, M., Podolske, J. R., Chan, K. R., and Gunson, M. R.: Evaluation of source gas lifetimes from stratospheric observations, Journal of Geophysical Research Atmospheres, 102, 25543–25564, https://doi.org/10.1029/97jd02215, 1997.

Wang, Y., Huang, D., Liu, J., Zhang, Y., and Zeng, L.: Alternative Environmentally Friendly Insulating Gases for SF$_6$, Processes, 7, https://doi.org/10.3390/pr7040216, 2019.